Optica Applicata, Vol. XXXIV, No. 1, 2004

Quantitative evaluation of 52 kD Ro/SS-A intracellular distribution in keratinocytes exposed to UVB radiation

ANNA WOŹNIACKA[1], KAROL LANGNER[2], DANIEL P. MCCAULIFFE[3], ANNA SYSA-JĘDRZEJOWSKA[1], MAREK LANGNER[2]

[1]Department of Dermatology, Medical University of Łódź, ul. Kremieniecka 5, 94-017 Łódź, Poland

[2]Institute of Physics, Wrocław University of Technology, Wybrzeże Wyspiańskiego 27, 50-370 Wrocław, Poland, e-mail: Marek.Langner@pwr.wroc.pl

[3]Department of Dermatology, University of North Carolina at Chapel Hill, Chapel Hill, North Carolina 27599-7287, USA

The intracellular location of the 52 kD Ro/SS-A autoantigen and its reaction upon stimuli are constantly subject to debate. One question still not resolved concerns the behavior of this protein following UVB irradiation. In order to monitor 52kD Ro/SS-A in time, the peptide was tagged with green fluorescence protein and over-expressed in keratinocytes. Evolution after UVB irradiation was observed using confocal fluorescence microscopy. By accepting a model that assumes the proportionality of pixel intensity to local green fluorescent protein (GFP) density, the distribution of the imaged protein in its relative density space can be calculated. Data analysis shows that the initial protein punctate structures located in the cytoplasm tend to disintegrate in a time-dependent manner. This agrees qualitatively with experimental evidence stating that the efficiency of immunological labeling is altered after UVB irradiation. Such dispersion must also co-exist with eventual enhanced exposure of 52 kD Ro/SS-A to the cell surface, which has been pointed out in the past by immunostaining experiments.

Keywords: autoantibodies, green fluorescent protein, Ro 52 kD/SS-A, histogram.

1. Introduction

Autoantibodies directed against the 52 kD and 60 kD Ro/SS-A autoantigens are found in the sera of patients with lupus erythematosus and disorders related to Sjogren's syndrome [1]–[6]. The cellular function of these autoantigens remains unclear and the precise intracellular location of the 52 kD Ro/SS-A autoantigen (Ro) has been subject to debate [7]–[10]. Initially, 52 kD Ro (52 Ro) was described to co-localize with the 60 kD Ro autoantigen in the nucleus [11]. More recent findings have challenged this notion by showing that 52 Ro is also cytoplasmic [9] and [10]. There have also been reports that the localizations of these two autoantigens are disparate [7] and [12]. In a

previous paper, we have demonstrated that besides faint diffuse cytoplasmic and nuclear distributions, 52 Ro localizes to discrete punctate structures (possibly aggregates) in the cytoplasm of epithelial cells [13].

Understanding the molecular configuration of Ro/SS-A ribonucleoprotein and its redistribution after such environmental stimuli as ultraviolet light is critical, especially for determining the molecular mechanisms of the disorders mentioned above [1] and [14]. It seems that autoantigens targeted in systemic lupus erythematosus cluster at the surface of apoptotic cells [15]. It has been shown using ELISA (enzyme-linked immunosorbent assay) and FACS (fluorescence-activated cell sorting) techniques that UVB irradiation induces the translocation of the whole Ro/SS-A RNP complex or its part to the cell surface of keratinocytes [16]–[18]. Calreticulin – a subfragment of Ro/SS-A RNP – has been reported to upregulate and express onto the plasma membrane surface of A431 cells after physiologically relevant doses of UVB radiation [19]. Both of these techniques provide limited and uncertain information on the cellular distribution of proteins. ELISA is suitable for finding the quantity of protein, however it provides no information concerning its intracellular distribution. On the other hand, FACS is able to detect only those proteins or their fragments that are exposed to the cell surface.

By using fluorescence confocal microscopy, which visualizes a selected protein in transgenic cells by tagging it with green fluorescence protein, pattern changes *in situ* can be followed. We have observed such changes after the UVB irradiation of keratinocytes expressing 52 Ro peptide tagged with green fluorescence protein. As in all imaging techniques, the sequences of images depicting cell colonies that were obtained in this study carry information that is to some extent noticeable but certainly not quantifiable to the unaided eye. Any casual observations of these are therefore necessarily subjective. In order to bring forth trends that are present in the sequences, we also performed a straightforward quantitative evaluation of them: a histometric analysis of the gathered fluorescence images. Concepts adopted for this analysis are described in detail in literature concerned with digital image evaluation [20] and [21].

2. Materials and methods

Keratinocyte transfection and irradiation conditions – A 431 cells (human keratinocyte cell line ATCC CRL-1555) were cultured in Dulbecco's modified Eagle's medium with 4.5 g/dm^3 of glucose and 10% fetal bovine serum according to recommended ATCC guidelines.

GFP transfection construct – A plasmid construct that encodes GFP fused to the carboxy-terminal end of the 52 Ro protein (pEGFP, Clontech Laboratories, Palo Alto, CA) was made. Utilizing Effectene transfection reagent this construct was transfected into A 431, according to the manufacturer's recommendations (Qiagen, Valencia, CA). Clones of the stable transfectants were established by culturing the modified A 431 cells in the presence of the neomycin/G18 selection marker (Gibco BRL Life Technologies, Grand Island, NY).

Irradiation of A 431 cell cultures – The cultured cells were irradiated in glass chamber slides without removing them from the growing medium. They received a dosage of 5 mJ/cm^2 UVB, emitted from Westinghouse FS 20 bulbs (with an emission spectra of 280–380 nm and peak at 313 nm). The UV dose and spectral distribution was determined by a radiometer (International Light, Newburyport, MA).

Digital image acquisition – The evolution of the transgenic keratinocytes irradiated with UVB was observed with a Zeiss 410 LSM microscope system with a 63X (N.A.1.4) plan Appl lens. The green fluorescence was excited at 488 nm with an argon laser and collected by a photomultiplier through a 515–530 nm band pass emission filter. Images were digitized to 8-bit grayscale format (768×512 pixels each) and stored on disc. Thus, each pixel holds an intensity value between 0 and 255. A control series was sampled in 15 time points, including an image corresponding to time-zero. The irradiated series was sampled 14 times, with no time-zero image. Since both series were registered in the same conditions, the control series can be treated as a time-zero reference.

Histometric analysis – The acquired images were analyzed from a histometric point of view. To this end, a matrix, in which each column was the grayscale intensity histogram of the respective image, was constructed. An element $G_{i,j}$ of this matrix denotes the amount of pixels of intensity i present in image j (in chronological order). The dimensions of matrix G are therefore 256 rows and 15 columns for the control series, and 256 rows and 14 columns for the irradiated series.

Considering that every pixel represents the same surface/volume element in the scanning plane and that grayscale intensity reflects linearly the amount of fluorescence energy registered from the appropriate area/volume, pixel intensity is proportional to local GFP density. Therefore, it is also proportional to the density of the protein tagged by GFP. Such an image model was accepted and is the basis for all further analysis.

The two matrices G were transformed in such a way as to hold cumulated pixel intensities with a progressive threshold, according to the formula

$$H_{i,j} = \sum_{k=i}^{255} k\, G_{k,j}.$$

Thus, an element $H_{i,j}$ is the sum of the grayscale intensities of all the pixels in image j with intensity above or equal to i. According to the accepted model, the elements $H_{i,j}$ also represent the relative amounts of protein that is more dense than a certain density corresponding to intensity i.

3. Results and discussion

Example images of the keratinocytes under study are presented in Fig. 1. The left column shows enhanced negatives of the control (Fig. 1**a**) and irradiated series after 40 (Fig. 1**b**), 300 (Fig. 1**c**) and 660 (Fig. 1**d**) minutes. The right column depicts negative binarized versions of the left column with a threshold of 80 – pixels with intensities

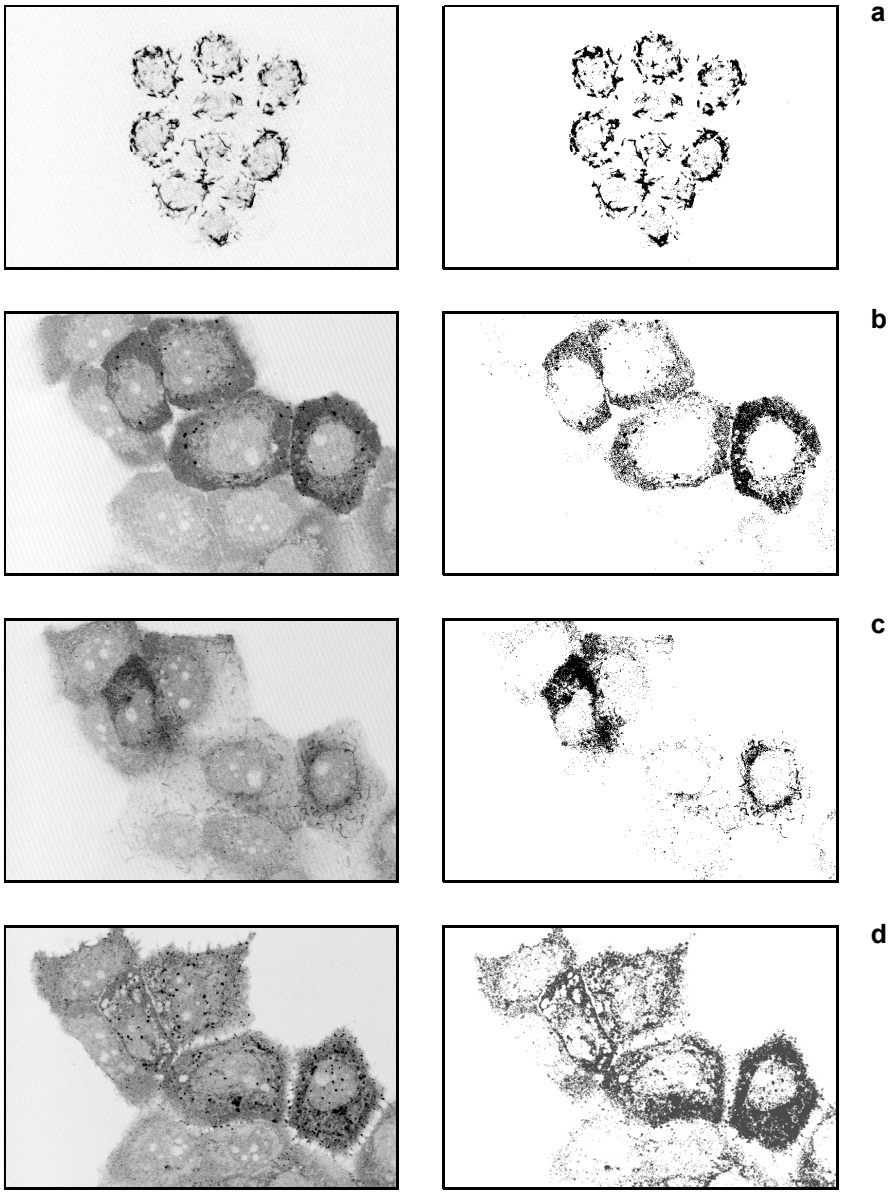

Fig. 1. Images of the control (**a**) and irradiated series after 40 (**b**), 300 (**c**), 660 (**d**) minutes. The left column shows enhanced greyscale negatives. The right column shows the binarized negatives of the left column with a threshold of 80.

below the threshold appear white, equal or above this threshold appear black. Unirradiated cells have a characteristic fluorescence pattern, namely the labeled protein is scattered throughout the cytoplasm in dense punctate structures, suggesting an aggregated state [13]. Thresholding images in the above manner allows objects of

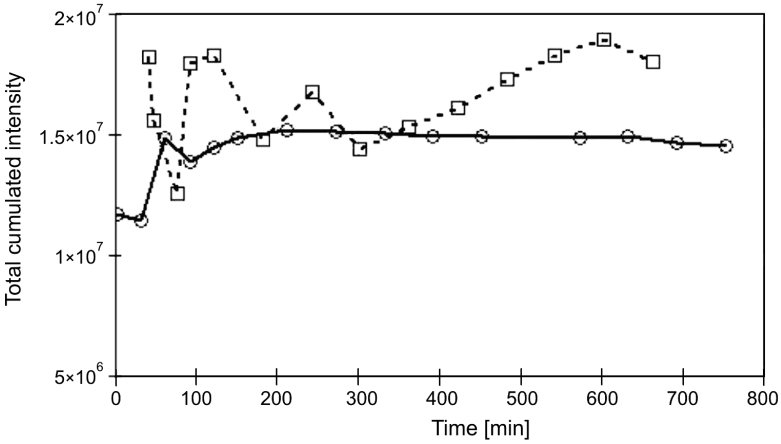

Fig. 2. Total cumulated pixel intensities for images in the control (circles, solid line) and irradiated (squares, dashed line) series.

fluorescence intensity above a given level to be selected. In terms of the accepted image model (pixel intensity is proportional to protein density), the right column of Fig. 1 shows only those points at which protein concentration is higher than a certain concentration corresponding to pixel intensity 80. This association allows the relative amount of peptide that is condensed above a chosen density to be measured by calculating the respective cumulated fluorescence intensity, *i.e.*, by summing up the intensities of all appropriate pixels, as in matrix H.

The total intensity of the control and irradiated images through time, taken as the matrix row $H_{0,j}$, is shown in Fig. 2. Such a parameter is known in image processing literature as integrated optical density (IOD) [20]. Within the accepted model, it is also proportional to the total amount of protein visible in the image. For the control series, it rises slightly during the first two hours and later remains level. In the irradiated series, it fluctuates somewhat, and grows systematically after 5 hours. No fluctuations exceed 50%.

Figure 3 shows a graphical representation of the matrix $H_{i,j}$ for the control (Fig. 3**a**) and irradiated (Fig. 3**b**) series. It is a systematic evaluation of cumulated pixel intensity for a progressive threshold in the form of a contour plot. Each point depicts a value for a given time and threshold, with lower values represented by darker regions. Values are proportional to GFP density, therefore these graphs show the cumulative distribution of protein in its relative density space (vertical intersections, parallel to the threshold axis) as a function of time. Values are plotted as double log values to visualize changes at high intensities. The density distribution is stable for the control series (Fig. 3**a**), which is reflected by parallel isodensity lines and by the symmetry in their fluctuations. The irradiated sample is qualitatively different, with isodensity lines changing in a more complex and nonsymmetric pattern. This indicates that after irradiation the character of protein distribution changes with time. If the protein forms aggregates, then the amount of aggregated peptide also must vary.

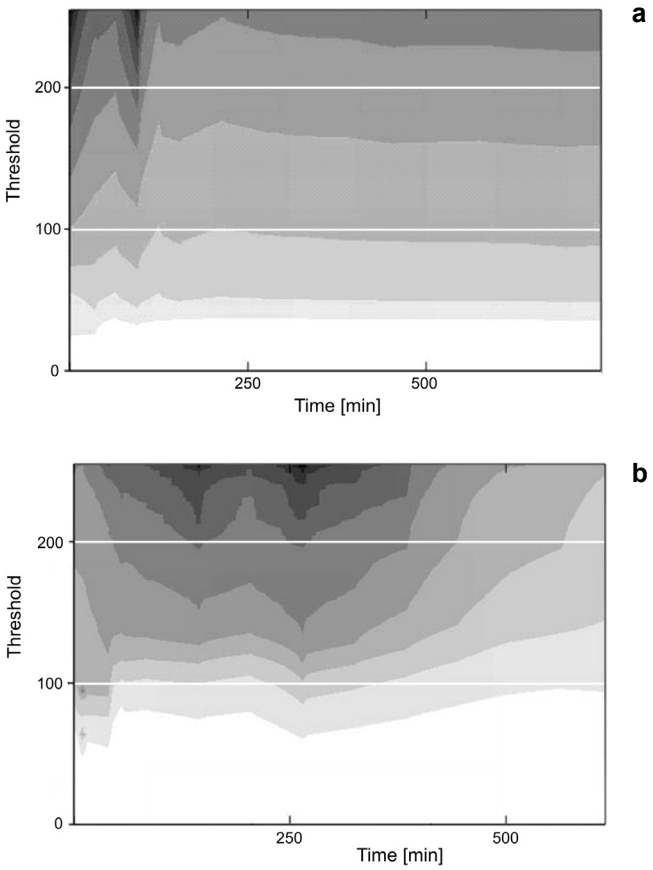

Fig. 3. Greyscale contour plots of cumulated pixel intensity with a progressive threshold for the control (**a**) and irradiated (**b**) series. Plotted values were linearly interpolated and logarithmized twice. Lower values are denoted by darker regions. The plots are intersected by two white lines each, representing constant threshold values of 100 and 200.

In order to quantify the difference between series in Fig. 3, cumulated pixel intensity as a function of time for two constant thresholds is compared in Fig. 4 for the control (Fig. 4**a**) and irradiated (Fig. 4**b**) series. In the matrix introduced previously, these traces are the rows $H_{100,j}$ and $H_{200,j}$. Thus, this figure presents the intersections drawn in Fig. 3 with horizontal white lines. Since density, according to the model, is a linear function $d(I)$ of pixel intensity I, then Fig. 4 shows how the amount of protein more dense than $d(100)$ and $d(200)$ changes with time. In the case of the control series (Fig. 4**a**), both fluctuate somewhat during the first two hours (in a symmetrical manner) and are further level. This corresponds to the stability pointed out for Fig. 3**a**. The evolution of the respective pair of traces for the irradiated series (Fig. 4**b**) is distinctly different. After approximately one hour, the amount of protein denser than $d(100)$ drastically grows by almost an order of magnitude, whereas that

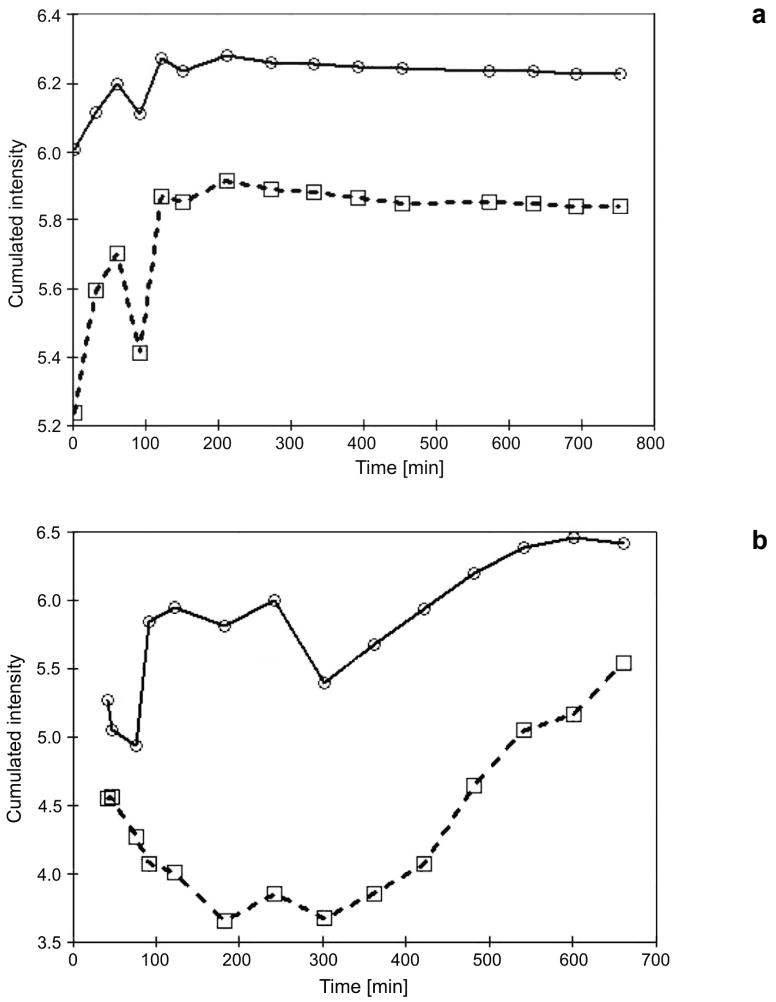

Fig. 4. Cumulated pixel intensity for the control (**a**) and radiated (**b**) series at two constant thresholds (the white lines in Fig. 3): 100 (circles, solid line) and 200 (squares, dashed line). The *x*-axis represents time, *y*-axis represents cumulated intensity in a logarithmic scale.

denser than $d(200)$ continues to fall. This redistribution of protein in its relative density space towards lower densities implies massive peptide dispersion and a breakdown of its punctate structures. After 300 minutes, both quantities start to rise.

To further demonstrate the extent of this phenomenon and to render it independent of the total amount of protein (demonstrated by IOD in Fig. 2), the ratio of the two traces in Fig. 4 is compared for both series in Fig. 5. Namely, the ratio is of cumulated pixel intensity for a threshold of 100 *vs.* that for a threshold of 200. In the matrix notation adopted, this is a vector with elements of the form $H_{100,j}/H_{200,j}$. This is also the ratio of the amount of protein denser than $d(100)$ *vs.* the amount denser than

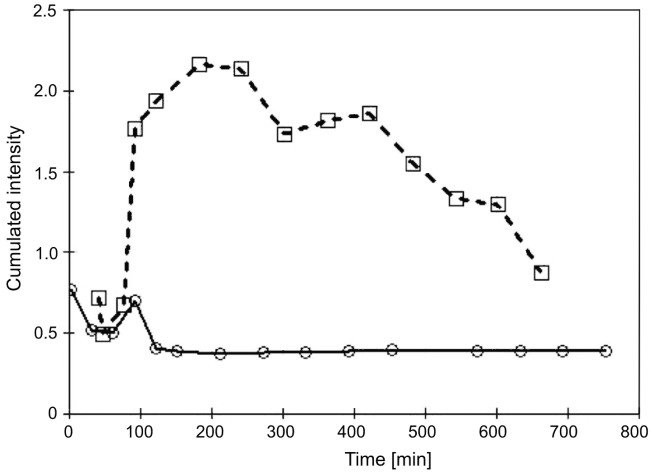

Fig. 5. Ratios of cumulated pixel intensity at a constant threshold of 100 *vs*. 200 (shown separately in Fig. 4), for the control (circle, solid line) and irradiated (squares, dashed line) series. The *x*-axis represents time, *y*-axis represents the ratio in a logarithmic scale.

d(200). The studied ratio is similar for both series within the first hour after insertion/irradiation, reflecting the initial similarity of samples. During this first hour, there is roughly three times as much protein of density above *d*(100) than *d*(200).

After about an hour, a sharp rise (beyond an order of magnitude) for the irradiated sample is observed. Again, this means that the dense punctate structures observed (possibly aggregates) disperse. The amount of protein accumulated in them reaches its lowest value approximately 2 hours after irradiation. After 5 hours this ratio starts to fall and almost reaches its initial level (that of the control series). This is accompanied by a systematic growth in total relative protein quantity (Fig. 2).

The above simple histometric analysis proves that 52 Ro protein, initially condensed in fluorescent-dense structures in keratinocytes, is dispersed to a more uniform spread within 2 hours upon irradiation and remains in such a state for at least 4 hours, after which the cells likely die. If, in fact, 52 Ro protein migrates to the cell surface after irradiation as reported in [16]–[18], it does not do so in an unchanged state. As shown in this paper, the processes triggered by UVB include the unaggregation of the protein considered. It is important to remember that this conclusion is valid specifically for the 52 Ro protein in the present system only. On the other hand, such an analysis is general in the sense that it can be used to draw conclusions of the same type from image sequences of various systems (not cells or after different stimulus) and that it is reasonable to expect similar results for systems with enough common features.

Also, histometric analysis is usually the starting point for a broader contemplation of any image model. In our case, the present analysis will be supplemented by a future

morphological analysis of the obtained images, which will reveal how the quantified dispersion is related with eventual outward molecular migration and/or other geometric evolution of the 52 Ro protein pattern in the cells under study.

Acknowledgments – This work was supported by the Fulbright Program, grant No. 503-114 from the Medical University of Łódź and by the Institute of Physics of the Wrocław University of Technology, Poland.

References

[1] BEN-CHETRIT E., Br. J. Rheumatol. **32** (1993), 396.
[2] MCCAULIFFE D.P., Lupus **6** (1997), 158.
[3] MCCAULIFFE D.P., WANG L., SATOH M., REEVES W.H., SMALL D., J. Rheumatol. **24** (1997), 860.
[4] SIBILIA J., Rev. Rhum. Engl. Ed. **65** (1998), 45.
[5] GORDON T.P., BOLSTAD A.I., RISCHMUELLER M., JONSSON R., WATERMAN S.A., Autoimmunity **34** (2001), 123.
[6] RHODES D.A., IHRKE G., REINICKE A.T., MALCHEREK G., TOWEY M., ISENBERG D.A., TROWSDALE J., Immunology **106** (2002), 246.
[7] KELEKAR A., SAITTA M.R., KEENE J.D., J. Clin. Invest. **93** (1994), 1637.
[8] PEEK R., VAN VENROOIJ W.J., SIMONS F., PRUIJN G., Clin. Exp. Rheumatol. **12** Suppl 11 (1994), S15.
[9] KEECH C.L., GORDON T.P., MCCLUSKEY J., J. Autoimmunity **8** (1995), 699.
[10] POURMAND N., BLANGE L., RINGERTZ N., PETTERSSON L., Autoimmunity **28** (1998), 225.
[11] BEN-CHETRIT E., CHAN E.K., SULLIVAN K.F., TAN E.M., J. Exp. Med. **167** (1988), 1560.
[12] YELL J.A., WANG L., YIN H., MCCAULIFFE D.P., J. Invest. Dermatol. **107** (1996), 622.
[13] MCCAULIFFE D.P., SWEENEY A., WOZNIACKA A., Cell. Mol. Biol. Lett. **8** (2003), 133.
[14] IOANNIDES D., GOLDEN B.D., BUYON J.P., BYSTRYN J.C., Arch. Dermatol. **136** (2000), 340.
[15] CASCIOLA-ROSEN L.A., ANHALT G., ROSEN A., J. Exp. Med. **179** (1994), 1317.
[16] LEFEBER W.P., NORRIS D.A., RYAN S.R., HUFF J.C., LEE L.A., KUBO M., BOYCE S.T., KOTZIN B.L., WESTON W.L., J. Clin. Invest. **74** (1984), 1545.
[17] FURUKAWA F., KASHIHARA-SAWAMI M., LYONS M.B., NORRIS D.A., J. Invest. Dermatol. **94** (1990), 77.
[18] JONES S.K., Br. J. Dermatol. **126** (1992), 546.
[19] KAWASHIMA T., ZAPPI E.G., LIEU T.S., SONTHEIMER R.D., Dermatology **189** Suppl 1 (1994), 6.
[20] OBERHOLZER M., OSTREICHER M., CHRISTEN H., BRUHLMANN M., Histochem. Cell Biol. **105** (1996), 333.
[21] JAIN B., *Digital Image Processing*, Springer-Verlag, Berlin Heidelberg 1997, pp. 73–93.

Received September 19, 2003
in revised form November 12, 2003